Distributed Conversion of Common Mode into Differential Mode Interference

Distributed Conversion of Common-Mode into Differential-Mode Interference

Paolo S. Crovetti, *Member, IEEE,* Franco Fiori, *Member, IEEE,*

***Abstract*—In this paper, the mechanisms that lead to the conversion of common mode RF interference into differential mode disturbances, which corrupt the information content of nominal signals and impair the operation of electronic systems, are investigated. To this purpose, distributed and lumped common mode-into-differential mode conversion mechanisms are discussed with reference to a simple test structure that can be analytically described. On the basis of the proposed analysis, the origin and the relative impact of such mechanisms is highlighted and the detrimental effect of distributed common mode-into-differential mode conversion on the effectiveness of differential RF interference suppressing filters is discussed. Theoretical predictions are compared with experimental results.**

***Index Terms*—Electromagnetic Compatibility (EMC), Electromagnetic Interference (EMI), Common Mode Interference, Differential Interference, EMI Filters.**

I. Introduction

WHILE the information content of electrical signals is usually related to differential mode (DM) voltages and currents, unwanted signals and electromagnetic interference (EMI) often give rise to common mode (CM) radio frequency (RF) disturbances on power and signal lines of electronic systems, whose amplitude can be orders of magnitude higher with respect to nominal DM signals. Even though electronic systems are designed to reject CM interference, such an interference can be converted into DM disturbances during propagation, thus degrading nominal signals and/or inducing system failures. As a consequence, the ability of an equipment to operate properly in an electromagnetically polluted environment is strongly related with the mechanisms that lead to the conversion of CM into DM interference and such mechanisms need to be properly taken into account when considering interference suppression techniques.

Common mode-into-differential mode (CM-DM) conversion mechanisms have been previously addressed in the literature with reference to EMI coupling in cables [1-2], printed circuit board (PCB) traces [3] and integrated interconnects [4]. Moreover, CM-DM conversion has been taken into account in microwave filter design [5], in RF measurements [6] and has been intensively investigated with reference to electromagnetic compatibility (EMC) compliance tests [7-12]. In previous works, however, the equipment undergoing CM excitation (equipment under test, EUT) is usually regarded as a *lumped* element and the propagation of CM interference and its conversion into DM disturbances *within* the EUT body, are not considered.

P.S. Crovetti and F.Fiori are with the Dept. of Electronics of the Politecnico di Torino, corso Duca degli Abruzzi, 24, I-10129, Torino, Italy e-mail: paolo.crovetti@polito.it.

In this paper, the mechanisms by which CM interference is converted into DM disturbances within an electronic system undergoing CM excitation are specifically addressed. To this purpose, lumped and distributed CM-DM conversion mechanisms in the EUT body are highlighted and their relative impact on RF interference (RFI) propagation is analyzed with reference to a simple test structure that is described in terms of a transmission line (TL) and of a multiconductor transmission line (MTL) model. On the basis of such models, it is also highlighted how the effectiveness of commonly employed RFI suppression techniques based on DM filters can be impaired by distributed CM-DM conversion. Model predictions are finally validated on the basis of the results of CM RF current injection measurements that have been performed on a test board.

The paper has the following structure: in Section II, the problem of relating EUT-level DM voltages to CM injected disturbances is stated in general terms and both distributed and lumped CM-DM conversion mechanisms are introduced. In Section III, CM-DM conversion is analyzed with reference to a test structure. To this purpose, a TL and an MTL model of such a test structure, highlighting distributed and lumped CM-DM conversion mechanisms, are proposed. Such models are considered in Section IV in order to discuss the causes and the effects of lumped and distributed CM-DM conversion in an equipment undergoing CM RF current injection through its wiring harness. In Section V, the experimental validation of model predictions is addressed. For this purpose, the results of CM RF current injection measurements performed on a board including the structure considered in the previous Sections are presented and compared with model predictions, highlighting the mechanisms discussed in this paper. Finally, in Section VI, some concluding remarks are drawn.

II. EUT-level Differential Mode and Common Mode Signal Propagation

In this Section, the propagation of CM and DM interference in a generic equipment undergoing CM RF excitation through its wiring harness is addressed. More specifically, the lumped and distributed mechanisms by which CM interference can be converted into DM disturbances are investigated and the possible description of such mechanisms in terms of electrical models is discussed. Finally, the impact of distributed CM-DM conversion on RFI suppression techniques based on DM filtering is highlighted.

A. Differential and Common-Mode Signal Propagation

A generic equipment (EUT) over a metal plane, as shown in Fig.1a, is now considered. Here, the metal ground plane is

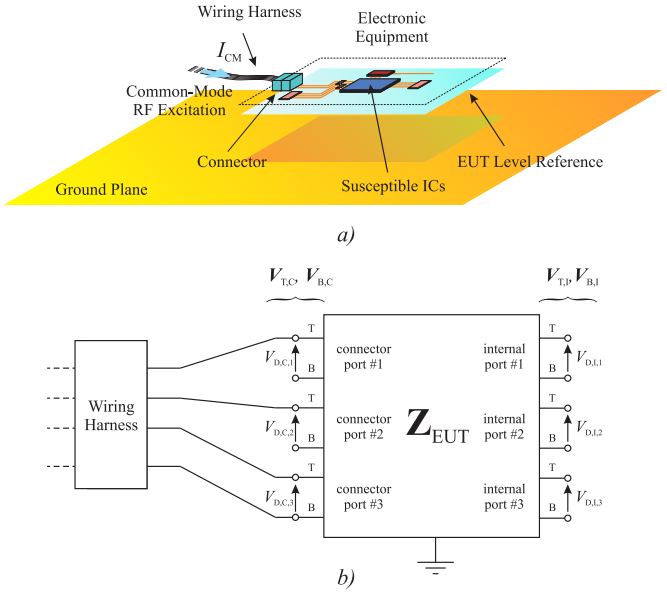

Fig. 1. Equipment Under Test undergoing common-mode RF excitation (a) and its complete model (b).

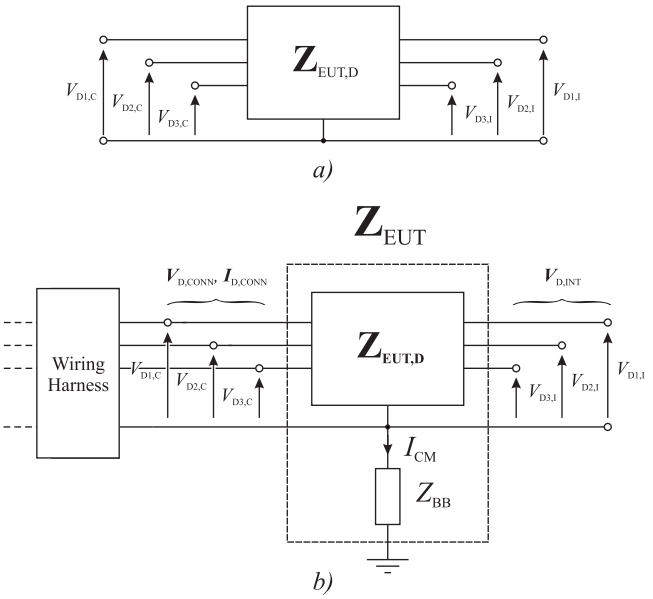

Fig. 2. Circuit models for the structure in Fig.1a valid for DM signal propagation (b) and simplified complete model based on the assumption of lumped CM-DM conversion (b).

conventionally assumed as the reference potential (*system reference* or *system ground*) and CM RF interference is injected into the wiring harness of the EUT. A reference conductor at the EUT level (*EUT reference* or *EUT ground*) is introduced as well and N EUT-level ports are defined with respect to such a reference. More precisely, each EUT-level port includes a top terminal taken on one non-reference conductor and a bottom terminal taken on the EUT reference conductor. An EUT reference conductor of arbitrary shape and electrical conductivity is now considered even though, in practice, it is usually made up of one or more PCB traces and/or wires, and/or metal patches and it often includes a full metal layer of a PCB (PCB ground plane), as depicted in Fig.1a.

The EUT in the setup of Fig.1a can be generally described in terms of the $2N$-port network in Fig.1b, which includes a system ground-referenced electrical port for each top and bottom terminal of the EUT. The electromagnetic behavior of the network in Fig.1b is fully specified by the impedance matrix $\mathbf{Z}_{\mathrm{EUT}}$, which relates voltages $\mathbf{V}_{\mathrm{EUT}}$ and currents $\mathbf{I}_{\mathrm{EUT}}$ at its $2N$ terminals. In such a matrix, the terminal voltages and currents can be labeled so that

$$\begin{pmatrix} \mathbf{V}_{\mathrm{T}} \\ \mathbf{V}_{\mathrm{B}} \end{pmatrix} = \begin{pmatrix} \mathbf{Z}_{\mathrm{TT}} & \mathbf{Z}_{\mathrm{TB}} \\ \mathbf{Z}_{\mathrm{BT}} & \mathbf{Z}_{\mathrm{BB}} \end{pmatrix} \begin{pmatrix} \mathbf{I}_{\mathrm{T}} \\ \mathbf{I}_{\mathrm{B}} \end{pmatrix} = \mathbf{Z}_{\mathrm{EUT}}\mathbf{I}_{\mathrm{EUT}} \quad (1)$$

in which the subscript B (bottom) refers to points on the EUT reference conductor and the subscript T (top) refers to points on other conductors of the EUT, and where vectors

$$\mathbf{V}_{\mathrm{T}} = \begin{pmatrix} \mathbf{V}_{\mathrm{T,c}} \\ \mathbf{V}_{\mathrm{T,i}} \end{pmatrix}, \ \mathbf{V}_{\mathrm{B}} = \begin{pmatrix} \mathbf{V}_{\mathrm{B,c}} \\ \mathbf{V}_{\mathrm{B,i}} \end{pmatrix},$$

$$\mathbf{I}_{\mathrm{T}} = \begin{pmatrix} \mathbf{I}_{\mathrm{T,c}} \\ \mathbf{I}_{\mathrm{T,i}} \end{pmatrix} \text{ and } \mathbf{I}_{\mathrm{B}} = \begin{pmatrix} \mathbf{I}_{\mathrm{B,c}} \\ \mathbf{I}_{\mathrm{B,i}} \end{pmatrix}$$

include voltages and currents in correspondence of the P EUT connector ports (subscript c) and in correspondence of the $Q = N - P$ internal EUT ports (subscript i), which can be associated to the input ports of integrated circuits.

As far as the DM voltages $\mathbf{V}_{\mathrm{D}}$ at the EUT ports are concerned, i.e. the voltages between each top node and the corresponding bottom node of the EUT-level reference, equation (1) can be written as

$$\mathbf{V}_{\mathrm{D}} = \mathbf{V}_{\mathrm{T}} - \mathbf{V}_{\mathrm{B}} = (\mathbf{Z}_{\mathrm{TT}} - \mathbf{Z}_{\mathrm{BT}})\,\mathbf{I}_{\mathrm{T}} + (\mathbf{Z}_{\mathrm{TB}} - \mathbf{Z}_{\mathrm{BB}})\,\mathbf{I}_{\mathrm{B}}. \quad (2)$$

Moreover, assuming a pure DM excitation, i.e. the current entering each top node equals the current exiting the corresponding bottom node, equation (2) can be further simplified as follows

$$\mathbf{V}_{\mathrm{D}} = (\mathbf{Z}_{\mathrm{TT}} + \mathbf{Z}_{\mathrm{BB}} - \mathbf{Z}_{\mathrm{TB}} - \mathbf{Z}_{\mathrm{BT}})\,\mathbf{I}_{\mathrm{D}} = \mathbf{Z}_{\mathrm{EUT,D}}\mathbf{I}_{\mathrm{D}} \quad (3)$$

where $\mathbf{I}_{\mathrm{D}} = \mathbf{I}_{\mathrm{T}} = -\mathbf{I}_{\mathrm{B}}$.

By comparing (1) and (3), it can be observed that $\mathbf{Z}_{\mathrm{EUT}}$ is a $2N \times 2N$ matrix, while $\mathbf{Z}_{\mathrm{EUT,D}}$ is an $N \times N$ matrix that provides all the information required to relate DM voltages and DM currents. As a consequence, as far as DM signal propagation is concerned, the EUT can be modeled without loss of generality by the N-port network in Fig.2a, in which all ports are referenced to the same terminal, that is conventionally associated to the EUT reference conductor. It should be noticed that the above discussion is completely general and does not rely on the assumption that the EUT reference is a good or an ideal conductor.

Electrical models for DM signal propagation, relating EUT-level DM port voltages and currents as described above, are usually derived for nominal EUT analysis and design and can be effectively extended to cover the whole EMI frequency range by adding proper parasitics. Unfortunately, however, a model derived under the hypothesis of DM signal propagation cannot be applied, in general, to discuss the behavior of the EUT in the presence of a CM excitation. In this case, in fact, some of the current $\mathbf{I}_{\mathrm{T}}$ (or $\mathbf{I}_{\mathrm{B}}$) is diverted to the system ground, $\mathbf{I}_{\mathrm{T}} \neq -\mathbf{I}_{\mathrm{B}}$, equation (3) cannot be applied and the

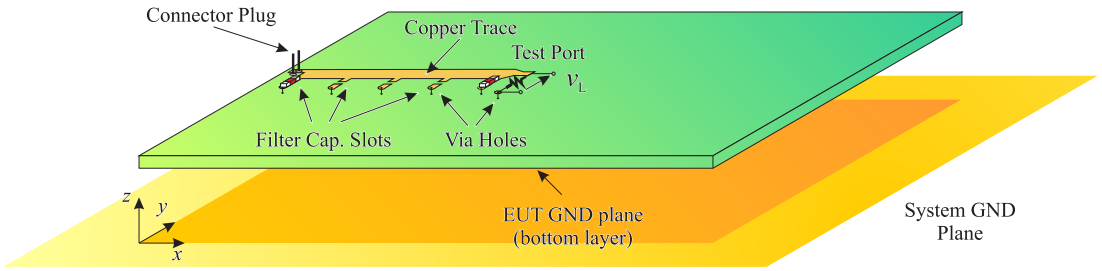

Fig. 3. Test structure that is considered in order to investigate CM-DM conversion.

EUT should be analyzed by the $2N$-port network in Fig.1b, whose $\mathbf{Z}_{\rm EUT}$ matrix needs to be extracted on the basis of a full-wave electromagnetical model of the EUT in its test environment.

B. Lumped Vs. Distributed CM-DM Conversion

Even though the $2N$-port network in Fig.1b should be rigorously considered in order to analyze an EUT in the presence of CM excitation, such a network can be significantly simplified under the assumption that the EUT reference conductor is equipotential and that top ports are not directly coupled to the system ground. Under the above hypotheses, in fact

$$\mathbf{Z}_{\rm BB} = \mathbf{Z}_{\rm BT} = \mathbf{Z}_{\rm TB} = Z_{\rm BB}\mathbf{U}_{NN} \tag{4}$$

where $\mathbf{U}_{AB}$ is an $A\times B$ matrix whose elements are all ones, as it is shortly demonstrated in Appendix A. Taking into account of (4), (1) takes the form

$$\begin{pmatrix} \mathbf{V}_{\rm T} \\ \mathbf{V}_{\rm B} \end{pmatrix} = \begin{pmatrix} \mathbf{Z}_{\rm TT} & Z_{\rm BB}\mathbf{U}_{NN} \\ Z_{\rm BB}\mathbf{U}_{NN} & Z_{\rm BB}\mathbf{U}_{NN} \end{pmatrix} \begin{pmatrix} \mathbf{I}_{\rm T} \\ \mathbf{I}_{\rm B} \end{pmatrix} \tag{5}$$

and, by the change of variables illustrated in Appendix B, it can be expressed in terms of DM and CM quantities as

$$\begin{pmatrix} \mathbf{V}_{\rm D} \\ V_{\rm B} \end{pmatrix} = \begin{pmatrix} \mathbf{Z}_{\rm EUT,D} & \mathbf{0}_{N1} \\ \mathbf{0}_{1N} & Z_{\rm BB} \end{pmatrix} \begin{pmatrix} \mathbf{I}_{\rm D} \\ I_{\rm CM} \end{pmatrix} \tag{6}$$

where bottom ports are merged in a single bulk port, $\mathbf{0}_{AB}$ is an $A \times B$ matrix whose elements are all zeros and

$$I_{\rm CM} = \sum_{i=1}^{N} \left(I_{{\rm T},i} + I_{{\rm B},i} \right). \tag{7}$$

On the basis of (6), the $2N$-port network in Fig.1b can be reduced to an $(N+1)$-port network as depicted in Fig.2b, where the current $I_{\rm CM}$ defined in (7) flows in $Z_{\rm BB}$. Moreover, the same matrix $\mathbf{Z}_{\rm EUT,D}$ defined in (3), that describes DM signal propagation and is easily obtained by standard extraction techniques, can be directly employed in (6) to analyze an EUT undergoing CM excitation.

Since (6) can be expressed in terms of connector and internal voltages and currents as

$$\begin{pmatrix} \mathbf{V}_{\rm D,c} \\ \mathbf{V}_{\rm D,i} \\ V_{\rm b} \end{pmatrix} = \begin{pmatrix} \mathbf{Z}_{\rm EUT,D,cc} & \mathbf{Z}_{\rm EUT,D,ci} & \mathbf{0}_{P1} \\ \mathbf{Z}_{\rm EUT,D,ic} & \mathbf{Z}_{\rm EUT,D,ii} & \mathbf{0}_{Q1} \\ \mathbf{0}_{1P} & \mathbf{0}_{1Q} & Z_{\rm BB} \end{pmatrix} \begin{pmatrix} \mathbf{I}_{\rm D,c} \\ \mathbf{I}_{\rm D,i} \\ I_{\rm CM} \end{pmatrix},$$

assuming injection through the wiring harness (i.e. assuming $\mathbf{I}_{\rm D,i} = \mathbf{0}_{Q1}$) internal port DM voltages $\mathbf{V}_{\rm D,i}$ are expressed as

$$\mathbf{V}_{\rm D,i} = \mathbf{Z}_{\rm EUT,D,ic}\mathbf{I}_{\rm D,c} = \mathbf{Z}_{\rm EUT,D,ic}\mathbf{Z}^{-1}_{\rm EUT,D,cc}\mathbf{V}_{\rm D,c} \tag{8}$$

and depend only on the DM quantities $\mathbf{I}_{\rm D,c}$ and $\mathbf{V}_{\rm D,c}$ at the connector level.

As a consequence, as far as the above assumptions are valid, DM voltages at the internal ports of an EUT undergoing CM excitation depend only on the DM components (with respect to the EUT reference) of the injected interference, which arise at the EUT connector because of unbalance in the wiring harness termination [12] and CM-DM conversion can be regarded as a lumped phenomenon occurring in correspondence of the EUT connector, whereas the propagation of RFI from the connector to internal nodes follows the DM signal path.

When the hypotheses of (6) are not exactly met, however, CM interference is converted into DM disturbances both at the connector, by the same *lumped CM-DM conversion mechanism* highlighted above, and also by *distributed CM-DM conversion* in the whole EUT body.

The possibility of describing RFI propagation in an EUT undergoing CM RF excitation in terms of pure lumped CM-DM conversion has a remarkable impact on the effectiveness of RFI suppression techniques. With reference to (8), in fact, RFI at each internal port of the EUT is necessarily suppressed if DM interference at the connector is suppressed (i.e. if $\mathbf{V}_{\rm D,c} \simeq \mathbf{0}_{Q1}$) and/or if DM mode RF propagation from the connector to susceptible ports is attenuated by DM filters (i.e. if $\mathbf{Z}_{\rm D,EUT,ic} \simeq \mathbf{0}_{PQ}$ and/or $\mathbf{Z}_{\rm D,EUT,ic}\mathbf{Z}^{-1}_{\rm D,EUT,cc} \simeq \mathbf{0}_{PQ}$ in the interference bandwidth). On the contrary, if distributed CM-DM conversion is relevant, the effectiveness of DM filtering techniques could be impaired since CM interference could be translated into DM disturbances in the whole EUT body, reaching IC ports even in the presence of DM filters.

In the following, the propagation of RF interference and the conversion of CM interference into DM disturbances is addressed considering a specific test structure. With reference to such an example, the causes and the effects of lumped and distributed CM-DM conversion are highlighted and the impact of EMI suppression techniques on lumped and distributed CM-DM conversion is also discussed.

III. CM-DM Conversion in a Test Structure

The lumped and distributed mechanisms, which lead to the conversion of CM interference into EUT-level DM disturbances, are investigated in this paper with reference to a simple PCB structure. In this Section, the test structure is introduced and described in terms of two different TL models considering, in one case, both lumped and distributed CM-DM conversion

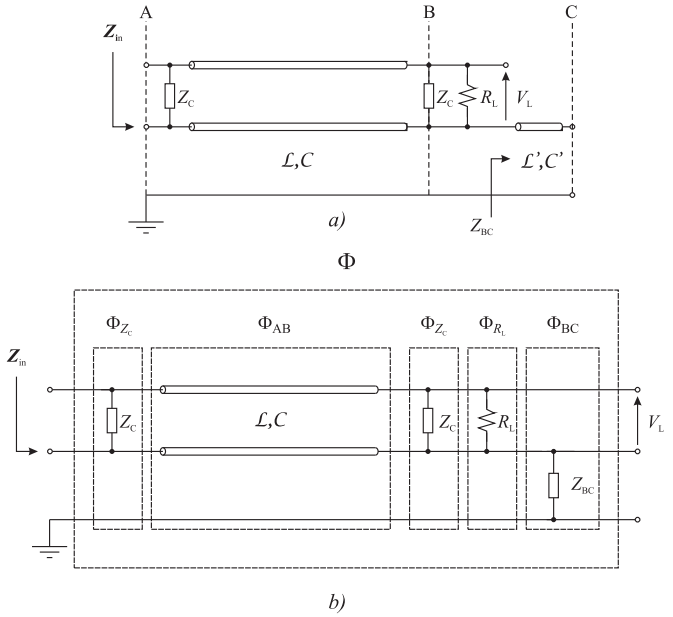

Fig. 4. Circuit model of the test board in Fig.3 derived taking into account of distributed CM/DM conversion (a) and its formulation in terms of ABCD parameters (b).

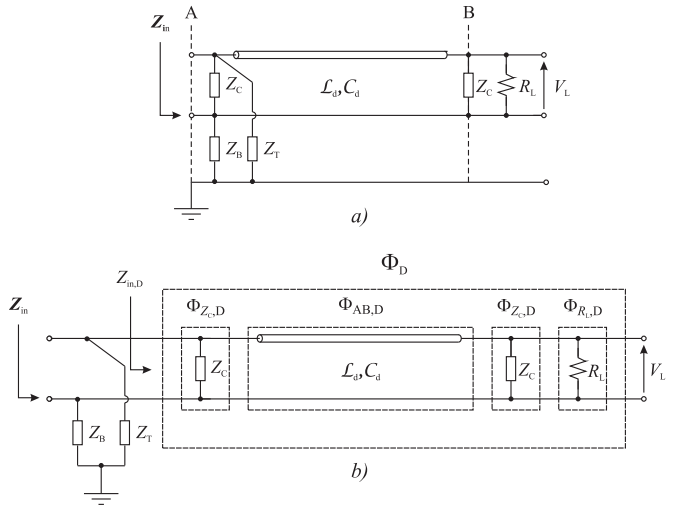

Fig. 5. Circuit model of the test board in Fig.3 derived under the assumption of lumped CM-DM conversion (a) and its formulation in terms of ABCD parameters (b).

and, in the other case, taking into account of lumped CM-DM conversion only, under the hypotheses of Section II.B.

A. PCB Test Structure

The $200\,\mathrm{mm} \times 100\,\mathrm{mm}$, two-layer, PCB depicted in Fig.3, with an FR-4 dielectric ($\varepsilon_\mathrm{r} = 4$) with a thickness of $1.6\,\mathrm{mm}$, placed $25\,\mathrm{mm}$ above a metal plane is considered in this paper as a test structure. Such a PCB includes a socket to be connected to a two-wire harness. One terminal of the socket is shorted to the PCB ground plane, which is extended over the whole bottom layer, while the other terminal is connected to one end of a $150\,\mathrm{mm}$-long, $5\,\mathrm{mm}$-wide copper trace on the PCB top layer, as shown in Fig.3. The other end of the trace is terminated on an $R_\mathrm{L} = 100\,\Omega$ resistor. Five slots for filter capacitors are located along the trace and each slot is connected to the PCB ground plane by a via hole.

The electrical length of the PCB trace over the PCB ground plane, described as a microstrip structure, is about $\frac{\ell}{\lambda} = 0.01$ at $f = 10\mathrm{MHz}$, nonetheless, when filter capacitors are introduced in the slots, the effective electrical length of the loaded microstrip structure is much higher ($\frac{\ell}{\lambda} = 0.8$ at $f = 10\,\mathrm{MHz}$ for two 100nF filter capacitors) and distributed effects may arise at frequencies below $10\,\mathrm{MHz}$.

The test board described above is subjected to CM RF excitation in correspondence of the wiring harness, and the prediction of the amplitude of RF disturbances, that are induced at the test port defined in correspondence of the resistor R_L, which stands for the input port of a susceptible IC, is addressed in the following. To this purpose, two different models of the test structure, taking into account fully distributed CM-DM conversion and considering only lumped CM-DM conversion, under the hypotheses of the previous Section, are now proposed. Then, the evaluation of the test port voltage V_L in terms of connector level excitation is addressed.

B. Test Structure Model Describing Distributed CM-DM Conversion

The derivation of an electromagnetic model fully describing distributed CM-DM conversion is, in general, a rather complex task that requires full-wave simulations. With reference to the simple test structure in Fig.3, however, such a derivation can be performed analytically in order to gain a deeper insight in the mechanisms that lead to CM-DM conversion.

The structure in Fig.3, in fact, can be described as a quasi-transverse electromagnetic (TEM) guiding structure in the x direction and it can be modeled in terms of TL theory, as shown in Fig.4 and Fig.5. More precisely, the PCB trace and the PCB ground plane can be modeled as an MTL over the system ground plane (section AB in Fig.4a and in Fig.5a), the PCB section from the RF detector to the edge can be modeled as a TL over the system ground plane (section BC in Fig.4a) and the termination resistor R_L, as well as filter capacitors Z_C, can be introduced in such a model as lumped elements.

The per-unit-length (p.u.l.) parameters of the MTL and of the TLs in Fig.4a and in Fig.5a can be extracted by solving the 2D Laplace equation with reference to the cross section of the structure in Fig.3 by an electromagnetic simulator, nonetheless, some considerations on p.u.l. parameters of the MTL AB and on their mutual relations, that provide further insight in CM-DM conversion, are presented in the following. Then, the test port voltage V_L is evaluated in terms of connector-level CM excitation.

1) Multi-Conductor Transmission Line AB Parameters: An outline on the derivation of the p.u.l. parameters of the MTL describing the section AB of the test structure in Fig.4a is presented in the following, in order to highlight if, and under what conditions, the hypotheses in Section II.B are verified in such an MTL. Both dielectric and conductor losses are

$$\mathbf{L} = \frac{1}{c}\mathbf{C_0}^{-1} = \frac{1}{c}\frac{1}{C_{0,\mathrm{TB}}\left(\mathcal{C}_{0,\mathrm{B}}+\mathcal{C}_{0,\mathrm{T}}\right)}\begin{pmatrix} \mathcal{C}_{0,\mathrm{TB}}+\mathcal{C}_{0,\mathrm{B}} & \mathcal{C}_{0,\mathrm{TB}} \\ \mathcal{C}_{0,\mathrm{TB}} & \mathcal{C}_{0,\mathrm{TB}}+\mathcal{C}_{0,\mathrm{T}} \end{pmatrix} \tag{9}$$

neglected in the following for the sake of simplicity[1].

The p.u.l. inductance matrix $\mathbf{L}$ of the MTL AB is evaluated in terms of the p.u.l. capacitance matrix $\mathbf{C_0}$ of the same structure in air (i.e. of a geometrically identical MTL embedded in an homogeneous dielectric with $\varepsilon_\mathrm{r} = 1$), as shown in (9) at the top of the page [13]. Here, c is the speed of light, $\mathcal{C}_{0,\mathrm{TB}}$ is the p.u.l. capacitance of the PCB trace over the PCB ground plane, $\mathcal{C}_{0,\mathrm{B}}$, is the p.u.l. capacitance of the PCB ground plane with respect to the system ground plane and $\mathcal{C}_{0,\mathrm{T}}$ is the p.u.l. direct coupling capacitance between the PCB trace and the system ground plane, which is much smaller than $\mathcal{C}_{0,\mathrm{TB}}$ and $\mathcal{C}_{0,\mathrm{B}}$ because of the shielding effect of the PCB ground plane. In the test structure of Fig.3, in particular, from numerical simulations, $\mathcal{C}_{0,\mathrm{T}}$ is about 4% of $\mathcal{C}_{0,\mathrm{TB}}$.

On the basis of equation (9), it follows that

$$\mathcal{C}_{0,\mathrm{T}} = 0 \quad \Rightarrow \quad \mathcal{L}_{12} = \mathcal{L}_{21} = \mathcal{L}_{22} = \frac{1}{c\,\mathcal{C}_{0,\mathrm{B}}},$$

i.e., if the p.u.l. direct coupling capacitance between the PCB trace and the system ground plane $\mathcal{C}_{\mathrm{T},0}$ is zero, the mutual inductance $\mathcal{L}_{21}$ is equal to the self inductance $\mathcal{L}_{22}$ and the PCB ground plane acts as an ideal shield [14]. As a consequence, the net DM voltage induced by a current flowing in the bottom conductor is zero and the first hypothesis for lumped CM-DM conversion formulated in Section II.B is exactly met.

The p.u.l. capacitance matrix $\mathbf{C}$ of the MTL AB can be expressed in terms of the p.u.l. capacitance of the PCB trace over the PCB ground plane, $\mathcal{C}_{\mathrm{TB}}$, of the p.u.l. capacitance of the PCB ground plane with respect to the system ground, $\mathcal{C}_{\mathrm{B}}$ and in terms of the p.u.l. direct coupling capacitance $\mathcal{C}_{\mathrm{T}}$ between the PCB trace and the system ground, all evaluated considering the PCB dielectric ($\varepsilon_\mathrm{r} = 4$), and takes the form

$$\mathbf{C} = \begin{pmatrix} \mathcal{C}_{\mathrm{T}}+\mathcal{C}_{\mathrm{TB}} & -\mathcal{C}_{\mathrm{TB}} \\ -\mathcal{C}_{\mathrm{TB}} & \mathcal{C}_{\mathrm{TB}}+\mathcal{C}_{\mathrm{B}} \end{pmatrix}. \tag{10}$$

It can be observed that, if $\mathcal{C}_{\mathrm{T}} = 0$, the top trace is not directly coupled to the system ground plane, and the second hypothesis of Section II.B is exactly met.

In conclusion, the test structure in Fig.3 satisfies both the hypotheses for lumped CM-DM conversion stated in Section II.B, provided that the direct coupling p.u.l. capacitances $\mathcal{C}_{0,\mathrm{T}}$ and $\mathcal{C}_{\mathrm{T}}$ are zero. On the basis of electromagnetic simulations, however, it has been observed that such capacitances are rather small (from 4% to 10% of $\mathcal{C}_{0,\mathrm{TB}}$ depending on the trace width and on its position in the board) but not zero. The effects of such coupling on CM-DM conversion will be highlighted in the following.

[1]The effect of losses can be taken into account in the following replacing the p.u.l. capacitance and inductance matrices $\mathbf{C}$ and $\mathbf{L}$ with the matrices $\mathbf{C}' = \mathbf{C} + \frac{\mathbf{G}}{j\omega}$ and $\mathbf{L}' = \mathbf{L} + \frac{\mathbf{R}}{j\omega}$ where the conductance matrix $\mathbf{G}$ and the resistance matrix $\mathbf{R}$ describe dielectric and conductor losses, respectively.

2) ABCD Matrix Modeling: The propagation of RF disturbances in the test structure undergoing BCI tests is now analyzed by MTL theory in terms of ABCD parameters, calculated on the basis of the p.u.l. parameters obtained above. By so doing, the top and bottom voltages (V_T, V_B) and currents (I_T, I_B) of the MTL at section $x = 0$ are expressed in terms of top and bottom voltages and currents at section $x = \ell$ as

$$\begin{pmatrix} V_\mathrm{T}(0) \\ V_\mathrm{B}(0) \\ I_\mathrm{T}(0) \\ I_\mathrm{B}(0) \end{pmatrix} = \underbrace{\begin{pmatrix} \mathbf{A} & \mathbf{B} \\ \mathbf{C} & \mathbf{D} \end{pmatrix}}_{\mathbf{\Phi}_{\mathrm{AB}}(\ell)} \begin{pmatrix} V_\mathrm{T}(\ell) \\ V_\mathrm{B}(\ell) \\ I_\mathrm{T}(\ell) \\ I_\mathrm{B}(\ell) \end{pmatrix} \tag{11}$$

where $\mathbf{\Phi}_{\mathrm{AB}}(\ell)$ is the 4×4 ABCD transmission matrix of the MTL [13].

Similarly, the transmission matrix $\mathbf{\Phi}_Z$ describing a lumped impedance Z between the top and the bottom layer is employed to include SMD filter capacitors ($\mathbf{\Phi}_{Z_\mathrm{C}}$) and the termination resistor R_L ($\mathbf{\Phi}_{R_\mathrm{L}}$) in the model. Moreover, the input impedance Z_{BC} of the TL describing section BC in Fig.4a is evaluated and included in the $\mathbf{\Phi}_{\mathrm{BC}}$ matrix.

The transmission matrix $\mathbf{\Phi}$ describing the structure in Fig.4 from the connector to the test port can be evaluated by multiplying the transmission matrices of the blocks evaluated above and highlighted in Fig.4b. For the structure in Fig.4b, which includes one filter capacitor at the connector and one filter capacitor at the test port, such a matrix takes the form

$$\mathbf{\Phi} = \mathbf{\Phi}_{Z_\mathrm{C}}\mathbf{\Phi}_{\mathrm{AB}}\left(\ell_{\mathrm{AB}}\right)\mathbf{\Phi}_{Z_\mathrm{C}}\mathbf{\Phi}_{R_\mathrm{L}}\mathbf{\Phi}_{\mathrm{BC}} \tag{12}$$

where ℓ_{AB} is the length of the AB trace. The matrix $\mathbf{\Phi}$ describing other filter capacitor configurations can be obtained in a similar way.

C. Test Structure Model Based on the Lumped CM-DM Conversion Assumption

Under the assumption of lumped CM-DM conversion, the model in Fig.5a is obtained for the test board in Fig.3. In such a model, PCB-level signal propagation is described by a single microstrip line over the PCB bottom layer, while the coupling between the PCB bottom layer and the system ground is taken into account by the impedance Z_B. Such an impedance, as well as the coupling impedance Z_T, which describes the direct coupling between the trace and the system ground, has been evaluated so that the input impedance matrix $\mathbf{Z}_{\mathrm{in}}$ of the circuit in Fig.5a is identical to the one of the circuit in Fig.4a. Provided that the test board is properly described by the model in Fig.4a, the model in Fig.5a is its best approximation under the hypothesis of lumped CM-DM conversion.

The above model can be formulated using standard TL analysis techniques. In particular, the 2×2 ABCD transmission matrix $\mathbf{\Phi}_\mathrm{D}$ describing DM signal propagation from the connector to the test port, as depicted in Fig.5b, can be evaluated by the same approach of Section III.B.2. Such an analysis,

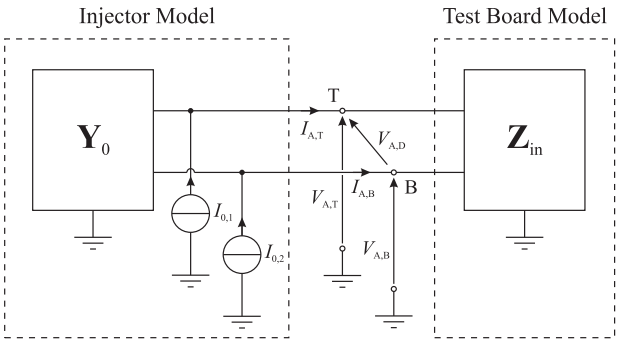

Fig. 6. Equivalent circuit for the evaluation of RF voltages and current at the connector of the test board.

however, is not reported here in further detail for the sake of conciseness.

D. Evaluation of the Test Port Voltage

The two models, that have been introduced so far, are now employed to evaluate the voltage $V_{\rm L}$ induced at the test port by RF interference injected through the wiring harness. To this purpose, it is now assumed that the injector, that provides CM RF excitation to the test structure at its connector, is described in terms of its Norton equivalent circuit, as depicted in Fig.6.

Since the input impedance matrix $\mathbf{Z}_{\rm in} = \mathbf{Y}_{\rm in}^{-1}$, which is seen at the connector of the test board, is the same when it is evaluated either by the distributed or by the lumped CM-DM conversion model introduced above, the connector voltages $\mathbf{V}_{\rm A} = (V_{\rm A,T}, V_{\rm A,B})^{\rm T}$ are the same according to both the two models and are expressed in terms of the admittance matrix $\mathbf{Y}_0$ and of the short-circuit current vector $\mathbf{I}_0 = (I_{0,1}, I_{0,2})^{\rm T}$ of the injector Norton equivalent as

$$\mathbf{V}_{\rm A} = \left(\mathbf{Y}_{\rm in} + \mathbf{Y}_0\right)^{-1} \mathbf{I}_0 = \mathbf{Z}\mathbf{I}_0. \tag{13}$$

Moreover, the vector $\mathbf{I}_{\rm A} = (I_{\rm A,T}, I_{\rm A,B})^{\rm T}$, including the currents which enter the test board, is given by

$$\mathbf{I}_{\rm A} = \mathbf{Y}_{\rm in}\mathbf{V}_{\rm A} = \mathbf{Y}_{\rm in}\mathbf{Z}\mathbf{I}_0. \tag{14}$$

From (13) and (14) it can be observed that, even if the injector is structurally symmetric (i.e. if $\mathbf{Y}_0$ is persymmetric, i.e. if $Y_{0,11} = Y_{0,22}$, $Y_{0,21} = Y_{0,12}$) the matrix $\mathbf{Z}$ is typically not persymmetric (i.e. $Z_{11} \neq Z_{22}$) since the coupling of the EUT-level ground plane towards the system ground is much higher with respect to the coupling of the trace to the system ground and $Y_{{\rm in},11} \neq Y_{{\rm in},22}$. As a consequence, under a pure CM excitation (i.e. for $I_{0,1} = I_{0,2} = \frac{I_0}{2}$), a DM voltage

$$V_{\rm A,D} = V_{\rm A,T} - V_{\rm A,B} = \left(Z_{11} - Z_{22}\right)\frac{I_0}{2} \tag{15}$$

and a DM current

$$I_{\rm A,D} = Y_{{\rm in},21}\left(Z_{11} - Z_{22}\right)\frac{I_0}{2} \tag{16}$$

are induced at the connector because of load unbalance. This mechanism gives rise to a *lumped CM-DM conversion* in correspondence of the connector, and is taken into account both by the distributed model and by the model derived under the assumption of lumped CM-DM conversion. According to the second model, however, no other CM-DM conversion mechanism is considered, while, according to the distributed model, conversion of CM interference into DM disturbances in the propagation from the connector to the test port is also considered. In order to highlight the impact of such a difference, the test port voltage $V_{\rm L}$ is now evaluated on the basis of the two models.

1) Distributed Model: The RF voltage $V_{\rm L}$ induced at the test port can be directly evaluated by the distributed CM-DM conversion model using the overall 4×4 transmission matrix $\mathbf{\Phi}$ describing RFI propagation from the connector to the test port. Considering the sub-matrices $\mathbf{A}$, $\mathbf{B}$, $\mathbf{C}$, $\mathbf{D}$ of $\mathbf{\Phi}$, the voltage vector $\mathbf{V}_{\rm B} = (V_{\rm B,T}, V_{\rm B,B})^{\rm T}$ at the section B of the structure in Fig.4 can be expressed in terms of the voltages at section A, evaluated in (13), as:

$$\mathbf{V}_{\rm B} = \mathbf{A}^{-1}\mathbf{V}_{\rm A} \tag{17}$$

and the test port voltage is therefore directly evaluated as

$$V_{\rm L} = V_{\rm B,T} - V_{\rm B,B}. \tag{18}$$

2) Model Derived under the Lumped CM-DM Conversion Assumption: According to the lumped CM-DM conversion model illustrated in Fig.5, no CM-DM conversion occurs in the propagation from the connector to the test port, as a consequence the voltage $V_{\rm L}$ is evaluated in terms of the DM voltage $V_{\rm A,D}$ induced at the connector calculated in (15), by using the 2×2 transmission matrix $\mathbf{\Phi}_{\rm D}$, which describes DM signal propagation along the PCB track AB. By this approach, the test port voltage is therefore evaluated as

$$V_{\rm L} = \frac{V_{\rm A,D}}{A_{\rm D}}, \tag{19}$$

where $A_{\rm D}$ is the (scalar) voltage transmission element in the ABCD matrix $\mathbf{\Phi}_{\rm D}$.

The above expressions are employed in the following to predict the voltage $V_{\rm L}$ at the test port of the board in Fig.3 and to discuss the impact of lumped and distributed CM-DM conversion in RFI propagation.

IV. Distributed vs. Lumped CM-DM Conversion

The causes and the effects of distributed and lumped CM-DM conversion are now discussed on the basis of the models derived so far. To this purpose, with reference to Fig.6, an ideal CM current injector for which $I_{0,1} = I_{0,2} = \frac{I_0}{2}$, $I_0 = 1\,{\rm A}$ and $\mathbf{Y}_0 = \mathbf{0}_{22}$ is assumed and the voltage $V_{\rm L}$ induced at the test port is calculated.

In Fig.7, such a voltage is evaluated, both by the distributed and by the lumped CM-DM conversion models, considering the test PCB in Fig.3 in which a filter capacitor C (with capacitance $100\,{\rm nF}$, parasitic series resistance ESR=$100\,{\rm m\Omega}$ and parasitic series inductance ESL = $3\,{\rm nH}$, including the inductance of the via hole to the ground plane) is placed in correspondence of the EUT connector. With reference to such a structure, different values of the p.u.l. direct coupling capacitance $\mathcal{C}_{0,\rm T}$ have been considered. More precisely, the cases of $\mathcal{C}_{0,\rm T} = \delta\,\mathcal{C}_{0,\rm TB}$ with $\delta = 0$, $\delta = 5\%$ and $\delta = 10\%$ are reported. While the first case corresponds to an idealized structure, the values considered in the second and in the

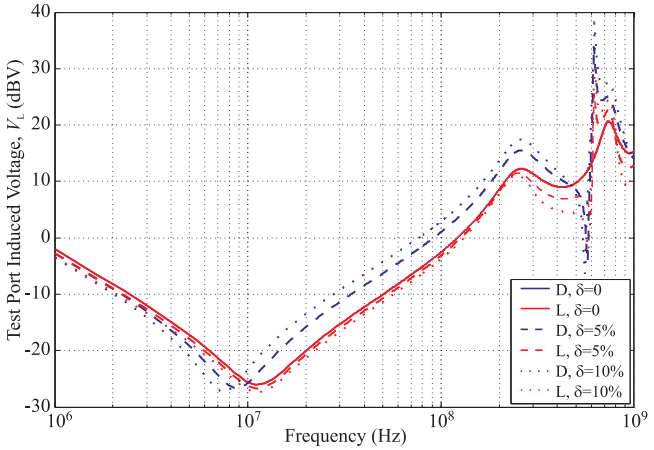

Fig. 7. Test port voltage V_{L} induced by a unitary CM current excitation at the connector of the test board in Fig.3, including one filter capacitor at the connector, evaluated by the full distributed (D) and by the lumped (L) CM-DM conversion model for different values of the ratio $\delta = \frac{C_{0,\mathrm{T}}}{C_{0,\mathrm{TB}}}$.

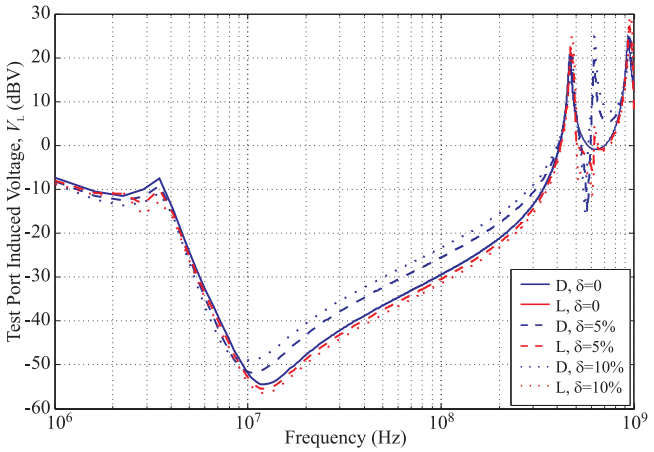

Fig. 8. Test port voltage V_{L} induced by a unitary CM current excitation at the connector of the test board in Fig.3, including two filter capacitors, evaluated by the full distributed (D) and by the lumped (L) CM-DM conversion model for different values of the ratio $\delta = \frac{C_{0,\mathrm{T}}}{C_{0,\mathrm{TB}}}$.

third example are similar to those obtained on the basis of electromagnetic simulations, considering the trace in the middle of the board and in proximity of an edge, respectively.

It can be observed that, according to the discussion in Section III, in the case of $\delta = 0$, the hypothesis of lumped CM-DM conversion is exactly met, therefore both the complete and the simplified model give the same results. For $\delta = 5\%$ and $\delta = 10\%$, instead, a difference of up to $5\,\mathrm{dB}$ between the predictions of the two models can be appreciated above $10\,\mathrm{MHz}$, where, according to the discussion in Section III.A, the effective electrical length of the microstrip structure loaded by the filter capacitor become relevant. Moreover, it can also be noticed that the introduction of such a very small direct coupling capacitance gives rise to a voltage peak at about $600\,\mathrm{MHz}$. Such a peak, which is related to direct coupling between the PCB trace and the system ground plane, is also highlighted (although underestimated by $7\,\mathrm{dB}$) by the lumped model considered in this paper, since it includes the direct

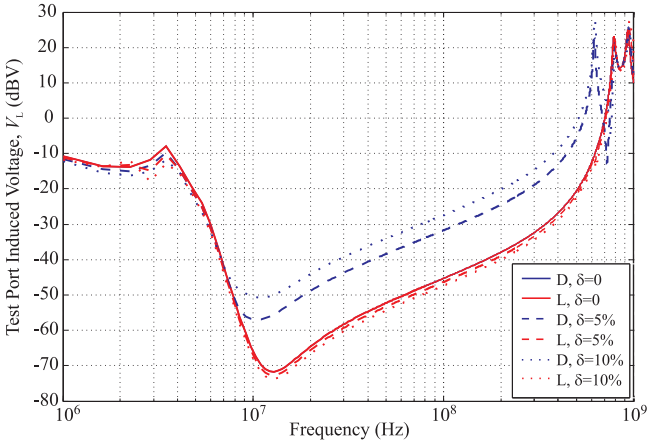

Fig. 9. Test port voltage V_{L} induced by a unitary CM current excitation at the connector of the test board in Fig.3, including three filter capacitors, evaluated by the full distributed (D) and by the lumped (L) CM-DM conversion model for different values of the ratio $\delta = \frac{C_{0,\mathrm{T}}}{C_{0,\mathrm{TB}}}$.

coupling impedance Z_{T} in Fig.5a. If such an impedance is neglected, as it is often done in practice, the lumped model prediction for $\delta = 5\%$ and $\delta = 10\%$ would be practically indistinguishable with respect to the case of $\delta = 0$ and the resonance at $600\,\mathrm{MHz}$ would not be highlighted.

In Fig.8 and Fig.9, the above analysis is repeated considering a test board with two identical filter capacitors in correspondence of the connector and of the test port (Fig.8) and three identical uniformly spaced filter capacitors (Fig.9). It can be observed that the discrepancy between the results obtained by the distributed and by the lumped models is of up to $10\,\mathrm{dB}$ in Fig.8 and more than $20\,\mathrm{dB}$ in Fig.9. Increasing the number of filter capacitors, in fact, the propagation of DM disturbances originated by lumped CM-DM conversion at the connector is strongly attenuated and distributed CM-DM conversion, not described by the lumped CM-DM model, becomes the dominant mechanism that translates injected interference into disturbances at IC ports.

From the above results it can be also observed how distributed CM-DM conversion impairs the effectiveness of DM filters. Comparing the curves in Fig.8 and Fig.9 evaluated for $\delta = 10\%$, for instance, it can be observed that the introduction of the third filter capacitor brings about an improvement in the suppression of RF interference at $100\,\mathrm{MHz}$ of only $2\,\mathrm{dB}$, from $-24\,\mathrm{dBV}$ to about $-26\,\mathrm{dBV}$. Taking only into account of the lumped CM-DM conversion only, one would have expected an enhancement of about $20\,\mathrm{dB}$, from $-28\,\mathrm{dBV}$ to $-48\,\mathrm{dBV}$.

V. Experimental Validation

The results about lumped and distributed CM-DM conversion mechanisms that have been discussed so far are now validated on the basis of CM RF current injection measurements. To this purpose, a devoted test board including the structure in Fig.3 has been put through CM RF current injection in order to measure the DM voltage induced at the test port by CM excitation. The measurement of such a voltage, however, is not a straightforward task since RF probes and/or RF cables and/or instruments connected to the test port affect CM signal

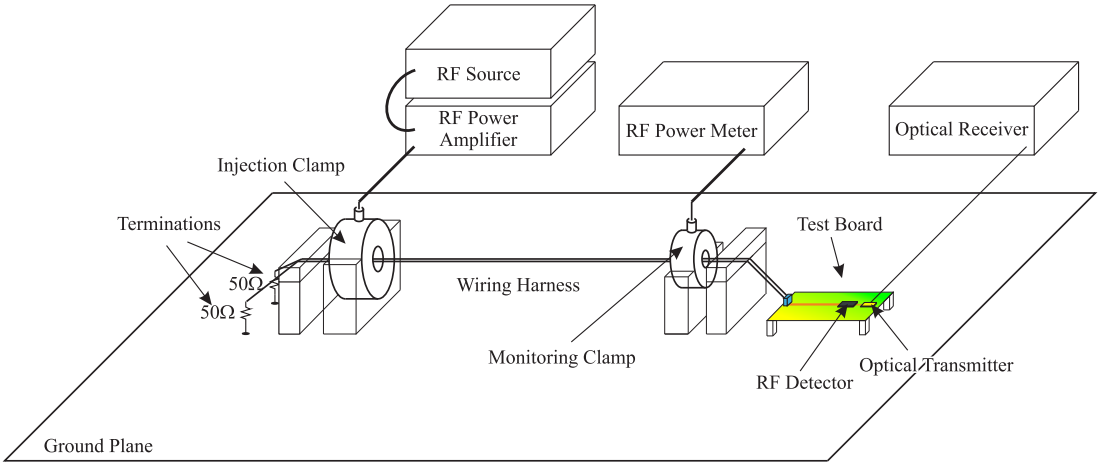

Fig. 10. Experimental Test Setup.

propagation and impair the significance of CM-DM conversion test results. In order to overcome such an inconvenience, an integrated RF meter has been placed directly on the test board and it has been connected to monitoring equipment by an optical fiber link, whose impact on the electromagnetic environment of the test is negligible.

In the following, the test board, the experimental setup and the test procedure, that are considered for validation, are firstly introduced. Then, model predictions and experimental results are compared and discussed.

A. Test Board, Test Setup and Test Procedure

A test board including the structure in Fig.3 has been fabricated to validate the results discussed in this paper. In such a board, the input terminals of an integrated RF-detecting circuit are located in correspondence of the test port in Fig.3. Such a device has a $100\,\Omega$ input impedance, equal to the termination resistance $R_{\rm L}$ considered in simulations, and it is sensitive to the root-mean-square (rms) value of the RF voltage applied to its input port in the bandwidth $50\,\mathrm{Hz}$-$3.8\,\mathrm{GHz}$ [15]. More precisely, such an RF detecting circuit has a digital output that changes its state whenever the rms value of the RF voltage applied to its input port exceeds $8\,\mathrm{mV}$, which corresponds, for a continuous wave (CW) signal, to a peak amplitude of about $11\,\mathrm{mV}$.

The digital output of the RF detecting circuit drives an optical transmitter that converts the information on the RF detector output state into an ON/OFF optical signal. The power supply voltage for the RF detector and for the transmitter circuit is provided by a battery that is located on the test board. Such a voltage is filtered by two $1\,\mu\mathrm{F}$ electrolytic capacitors and it is stabilized by an integrated low dropout regulator on the same test board.

The test setup that is schematically depicted in Fig.10 and which is similar to the one employed in Bulk Current Injection (BCI) susceptibility tests [7] is employed to perform CM RF current injection measurements on the test board. In such a setup, the socket of the test structure is connected to a $1\,\mathrm{m}$ long, two-wire harness running $50\,\mathrm{mm}$ above a copper plane. Each wire of the harness is terminated on a $50\,\Omega$ impedance towards the ground plane. Along the wiring harness, two RF clamps, i.e. the injection and the monitoring clamp, are located as depicted in Fig.10. The RF clamps F-130A-1 [16] and F-51 [17] by FCC are here employed as the injection and the monitoring clamp, respectively. The injection clamp is connected to the output of a $10\,\mathrm{W}$ RF power amplifier, whose input terminal is connected to a CW RF source, while the monitoring clamp is connected to an RF power meter to measure the injected CM RF current. The optical output of the test board, that has been described above, is connected to an optical fiber link which transmits the information of the RF detector output state to monitoring equipment out of the test area, without perturbing the electromagnetic environment.

With reference to the setup in Fig.10, a CW RF signal is generated by the RF source and amplified by the RF power amplifier so that an RF CM current is injected into the test board through the wiring harness. For each test frequency, the amplitude of the injected RF current is progressively increased until the RF detector logical output changes its state, i.e. until an RF CW signal with a peak amplitude higher $11\,\mathrm{mV}$ is induced on the test port. The threshold injected current $I^{\star}_{\rm CM}$ corresponding to such a condition is annotated for each frequency. If such a condition is not achieved for the maximum RF power deliverable by the amplifier, e.g. in correspondence of the wiring harness parallel resonances, in which a very low current is injected even though a high incident power is applied by the RF amplifier, no value is reported.

B. Model Predictions

On the basis of the results of CM RF current injection tests performed by the above procedure, a relation between RF voltages induced at the test port and injected CM current is experimentally established. Such a relation is now compared with the predictions obtained by the models introduced in this paper for validation. To this end, the parameters of the Norton equivalent circuit of the setup in Fig.6 are evaluated on the basis of scattering parameters measurements and are introduced in the models. The equivalent admittance matrix, in particular, is obtained by measuring the scattering matrix at

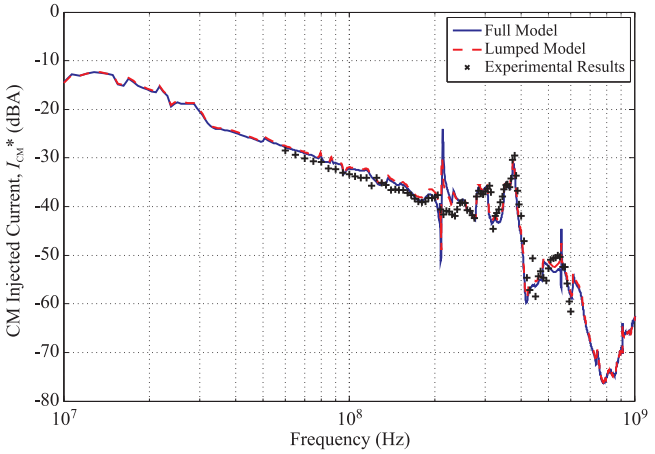

Fig. 11. Comparison of model predictions and experimental results: test board placed 25mm above system ground plane, with a single SMD filter capacitor ($C = 100\,\mathrm{nF}$, $\mathrm{ESR} = 100\,\mathrm{m\Omega}$, $\mathrm{ESL} = 3\,\mathrm{nH}$ including via hole inductance) located at the connector.

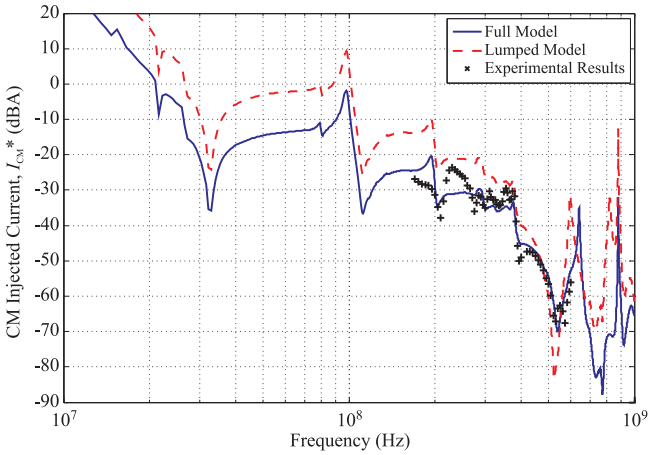

Fig. 12. Comparison of model predictions and experimental results: test board placed 25mm above system ground plane with two identical SMD filter capacitors ($C = 100\,\mathrm{nF}$, $\mathrm{ESR} = 100\,\mathrm{m\Omega}$, $\mathrm{ESL} = 3\,\mathrm{nH}$ including via hole inductance) located at the connector and at the test port.

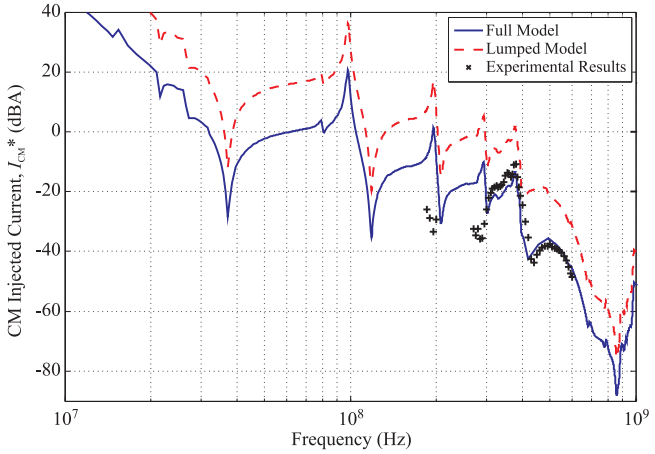

Fig. 13. Comparison of model predictions and experimental results: test board placed 25mm above system ground plane with three identical SMD filter capacitors ($C = 100\,\mathrm{nF}$, $\mathrm{ESR} = 100\,\mathrm{m\Omega}$, $\mathrm{ESL} = 3\,\mathrm{nH}$ including via hole inductance) located at the connector, at the test port and at the midpoint of the PCB trace from the connector to the test port.

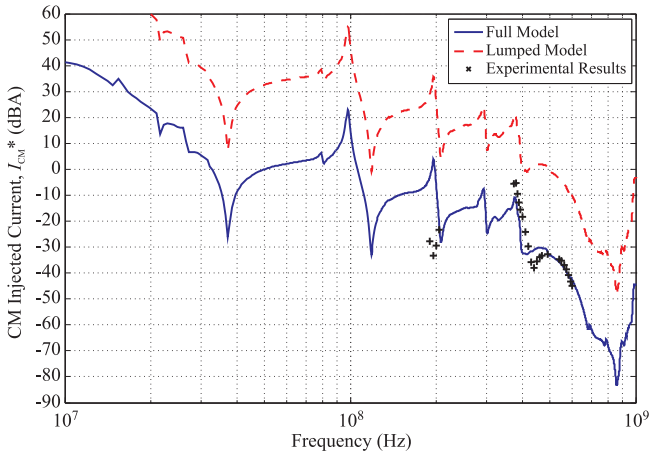

Fig. 14. Comparison of model predictions and experimental results: test board placed 25mm above system ground plane with five identical uniformly-spaced SMD filter capacitors ($C = 100\,\mathrm{nF}$, $\mathrm{ESR} = 100\,\mathrm{m\Omega}$, $\mathrm{ESL} = 3\,\mathrm{nH}$ including via hole inductance) .

the EUT connector of the wiring harness. Moreover, the short-circuit currents $I_{0,1}$ and $I_{0,2}$ appearing in Fig.6 are expressed, for the sake of symmetry, as

$$I_{0,1} = I_{0,2} = \frac{I_{\mathrm{CM}}}{2} \tag{20}$$

where I_{CM} is the CM injected current estimated from the voltage V_{meas} induced at the monitoring clamp by the calibration procedure described in [18].

On the basis of the test setup model described above and of the models presented in Section III, the injected current I_{CM} is related to the RF induced voltage V_{L} at the test port as

$$V_{\mathrm{L}} = Z_{\mathrm{T}} I_{\mathrm{CM}} \tag{21}$$

where Z_{T} can be evaluated by the distributed or by the lumped CM-DM conversion model by (18) or (19), respectively.

Since the logical output of the RF detector employed in tests changes its state whenever the test voltage V_{L} exceeds the threshold $V_{\mathrm{L}}^{\star} = 11\,\mathrm{mV}$, the injected current $I_{\mathrm{CM}}^{\star}$ that corresponds to such a condition can be evaluated as

$$I_{\mathrm{CM}}^{\star} = \frac{V_{\mathrm{L}}^{\star}}{Z_{\mathrm{T}}}. \tag{22}$$

The values of the threshold current $I_{\mathrm{CM}}^{\star}$ obtained by (22) are compared with the results of experimental CM RF current injection tests in the following.

C. Experimental Results

The measured threshold current $I_{\mathrm{CM}}^{\star}$ obtained by the CM RF current injection test carried out on the board in Fig.3 in the bandwidth 10 MHz-600 MHz as described above, is now compared with the predictions obtained by (22) in the bandwidth 10 MHz-1 GHz, on the basis of the models introduced in Section III.

To this purpose, the current $I_{\mathrm{CM}}^{\star}$ is plotted in Fig.11 for the test board including one filter capacitor at the connector. It can be observed that, in this case, the predictions obtained by

the full model in Fig.4 and by the model in Fig.5, derived under the hypothesis of lumped CM-DM conversion, are substantially similar and are both in reasonable agreement with experimental results. On the basis of the analysis proposed in this paper, the substantial agreement of full and lumped model predictions can be related to the fact that the DM interference suppression provided by a single filter capacitor is not very high and the propagation of RF interference to the test port is mainly related to lumped CM-DM conversion at the connector.

In Fig.12, the same comparison is proposed for a test board including one filter capacitor in correspondence of the connector and one filter capacitor in correspondence of the test port. It can be observed that the predictions obtained under the hypothesis of lumped CM-DM conversion differ of up to $10\,\mathrm{dB}$ from the predictions obtained by the full model, which is in significantly better agreement with experimental results. On the basis of the previous discussion, DM signal attenuation has been increased by the second filter capacitor and the contribution of distributed CM-DM conversion is no longer negligible. As a consequence, the additional RFI suppression provided by the second filter capacitor is less than expected on the basis of DM signal propagation only.

In Fig.13, the results of tests carried out on the same board including three uniformly spaced filters are shown. With reference to Fig.13, the predictions obtained under the hypothesis of lumped CM-DM conversion deviate of up to $20\,\mathrm{dB}$ from the predictions obtained by the full model, which is in agreement with experimental data. In this case, DM signal attenuation is further increased by the third filter capacitor and the contribution of distributed CM-DM conversion is now dominant. As a consequence, the RFI suppression provided by the third filter capacitor is much less than expected on the basis of DM signal propagation only.

Finally, in Fig.14, the test board including five uniformly-spaced capacitors is considered. It can be observed that, in this case, the predictions obtained under the hypothesis of lumped CM-DM conversion deviate of more than $30\,\mathrm{dB}$ from experimental results and from the predictions obtained by the full distributed model. By comparing Fig.14 and Fig.13, in particular, it can be observed that the two filter capacitors that have been added have brought about no further RFI suppression since RFI propagation to the test port is now completely related to distributed CM-DM conversion, which is not affected by DM filtering.

VI. Conclusion

The propagation of RF disturbances in an electronic equipment in the presence of CM RF excitation has been investigated and the lumped and distributed mechanisms leading to the conversion of CM injected interference into DM disturbances, which corrupt nominal signals and may induce system failures, have been highlighted. To this purpose, the impact of distributed and lumped CM-DM conversion has been discussed with reference to a simple test structure, for which both mechanisms can be analytically described in terms of TL and MTL models. On the basis of this analysis, it has been highlighted that distributed CM-DM conversion mechanisms can be dominant whenever DM RF signal propagation is strongly attenuated by RFI suppression filters. As a consequence, distributed CM-DM conversion impairs the effectiveness of DM filtering techniques in improving the immunity of an equipment to RF interference. Moreover, the actual immunity level of an equipment in which distributed CM-DM conversion is relevant, cannot be properly assessed on the basis of models derived under the assumption of lumped CM-DM conversion.

Experimental results obtained with reference to a test board undergoing CM RF current injection have been compared with the predictions obtained by models describing distributed and lumped CM-DM conversion. Measured results are in substantial agreement with model predictions and confirm the above considerations on the impact of lumped and distributed CM-DM conversion mechanisms in an electronic equipment undergoing CM RF excitation.

Appendix A

The properties of the $\mathbf{Z}_{\mathrm{EUT}}$ matrix describing the EUT in Fig.1 under the hypotheses that the EUT reference conductor is equipotential and that top nodes are not directly coupled to the system ground plane are now discussed. To fix the ideas, a possibly non-reciprocal, two-port ($N = 2$) EUT satisfying the above hypotheses is represented in Fig.15.

Under the hypothesis formulated above, the voltages of bottom nodes $\mathbf{V}_{\mathrm{B}}$, evaluated with respect to the system reference, are all equal. Hence, a test current injected into any bottom node gives rise to equal voltages at all bottom nodes and

$$\mathbf{Z}_{\mathrm{BB}} = Z_{\mathrm{BB}}\mathbf{U}_{NN}. \tag{23}$$

In order to evaluate the elements in the $\mathbf{Z}_{\mathrm{BT}}$ block, a test current is applied between the system ground and one top terminal, keeping other ports open. Since top terminals are not directly coupled to the system ground plane, only bottom ports provide a path to the system ground for the test current. Being bottom ports equipotential for hypothesis (i.e. they are equivalent to a single port) and taking into account of (23), it follows that

$$\mathbf{Z}_{\mathrm{BT}} = Z_{\mathrm{BB}}\mathbf{U}_{NN}. \tag{24}$$

With reference to Fig.15, in particular, a test current applied to any top terminal necessarily flows through the Z_{BB} impedance and (24) is therefore verified.

Finally, under the assumption that top terminals are not directly coupled to the system ground plane, the elements $\mathbf{Y}_{\mathrm{TT}}$ and $\mathbf{Y}_{\mathrm{TB}}$ of the admittance matrix $\mathbf{Y}_{\mathrm{EUT}} = {\mathbf{Z}_{\mathrm{EUT}}}^{-1}$ are related so that $\mathbf{Y}_{\mathrm{TB}} = -\mathbf{Y}_{\mathrm{TT}}$ hence

$$\mathbf{I}_{\mathrm{T}} = \mathbf{Y}_{\mathrm{TT}}\mathbf{V}_{\mathrm{T}} + \mathbf{Y}_{\mathrm{TB}}\mathbf{V}_{\mathrm{B}} = \mathbf{Y}_{\mathrm{TT}}\mathbf{V}_{\mathrm{D}}.$$

As a consequence

$$\mathbf{I}_{\mathrm{T}} = \mathbf{0}_{N1} \quad \Leftrightarrow \quad \mathbf{V}_{\mathrm{D}} = \mathbf{0}_{N1}. \tag{25}$$

Taking into account of equation (25), for any excitation $\mathbf{I}_{\mathrm{EUT}} = (\mathbf{0}_{1N}, \mathbf{I}_{\mathrm{B}})^{\mathrm{T}}$, in which $\mathbf{I}_{\mathrm{T}} = \mathbf{0}_{N1}$ it follows that

$$\mathbf{V}_{\mathrm{D}} = \mathbf{Z}_{\mathrm{TB}}\mathbf{I}_{\mathrm{B}} - \mathbf{Z}_{\mathrm{BB}}\mathbf{I}_{\mathrm{B}} = (\mathbf{Z}_{\mathrm{TB}} - \mathbf{Z}_{\mathrm{BB}})\,\mathbf{I}_{\mathrm{B}} = \mathbf{0}_{N1}. \tag{26}$$

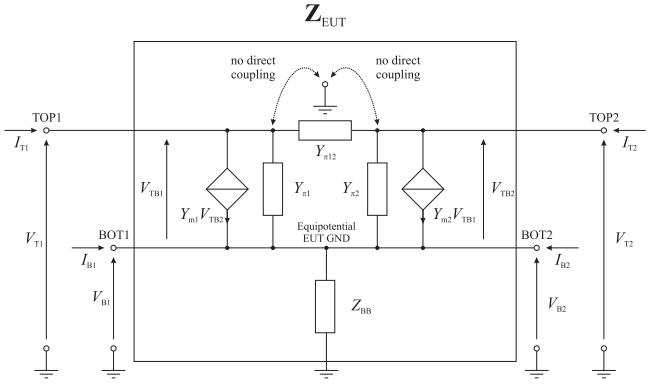

Fig. 15. Two-Port EUT Structure satisfying lumped CM-DM conversion hypotheses.

Since equation (26) must be valid for any $\mathbf{I}_{\rm B}$, it should be

$$\mathbf{Z}_{\rm TB} = \mathbf{Z}_{\rm BB}. \tag{27}$$

With reference to Fig.15, since controlled sources are driven by DM quantities[2], it can be observed that for a bottom test current excitation, no current flows through the elements between top and bottom nodes and (27) is therefore verified.

On the basis of (23), (24) and (27), the relations in (4) in the text are demonstrated under the hypotheses of Section II.B.

APPENDIX B

Since DM and CM quantities in equation (5) in the text are related to top and bottom quantities as

$$\begin{pmatrix} \mathbf{V}_{\rm D} \\ \mathbf{V}_{\rm B} \end{pmatrix} = \mathbf{P} \begin{pmatrix} \mathbf{V}_{\rm T} \\ \mathbf{V}_{\rm B} \end{pmatrix} \text{ and } \begin{pmatrix} \mathbf{I}_{\rm D} \\ \mathbf{I}_{\rm CM} \end{pmatrix} = \mathbf{Q} \begin{pmatrix} \mathbf{I}_{\rm T} \\ \mathbf{I}_{\rm B} \end{pmatrix},$$

where

$$\mathbf{P} = \begin{pmatrix} \mathbf{1}_N & -\mathbf{1}_N \\ \mathbf{0}_{NN} & \mathbf{1}_N \end{pmatrix} \quad \text{and} \quad \mathbf{Q} = \begin{pmatrix} \mathbf{1}_N & \mathbf{0}_{NN} \\ \mathbf{1}_N & \mathbf{1}_N \end{pmatrix},$$

in which $\mathbf{1}_N$ is the $N \times N$ identity matrix, from equation (1) it follows that

$$\mathbf{P}\mathbf{V}_{\rm EUT} = \mathbf{P}\mathbf{Z}_{\rm EUT}\mathbf{Q}^{-1}\mathbf{Q}\mathbf{I}_{\rm EUT}. \tag{28}$$

On the basis of (28), equation (5) in the text gives

$$\begin{pmatrix} \mathbf{V}_{\rm D} \\ \mathbf{V}_{\rm B} \end{pmatrix} = \begin{pmatrix} \mathbf{Z}_{\rm TT} - Z_{\rm BB}\mathbf{U}_{NN} & \mathbf{0}_{NN} \\ \mathbf{0}_{NN} & Z_{\rm BB}\mathbf{U}_{NN} \end{pmatrix} \begin{pmatrix} \mathbf{I}_{\rm D} \\ \mathbf{I}_{\rm CM} \end{pmatrix}$$

and, taking into account of the definition of the $\mathbf{Z}_{\rm EUT,D}$ in equation (3) in the text, as

$$\begin{pmatrix} \mathbf{V}_{\rm D} \\ \mathbf{V}_{\rm B} \end{pmatrix} = \begin{pmatrix} \mathbf{Z}_{\rm EUT,D} & \mathbf{0}_{NN} \\ \mathbf{0}_{NN} & Z_{\rm BB}\mathbf{U}_{NN} \end{pmatrix} \begin{pmatrix} \mathbf{I}_{\rm D} \\ \mathbf{I}_{\rm CM} \end{pmatrix}. \tag{29}$$

Finally, since the rows and the columns from $N+1$ to $2N$ of the matrix are all equal, equation (29) can be written as shown in equation (6) in the text, where

$$I_{\rm CM} = \mathbf{U}_{N1}\mathbf{I}_{\rm CM} = \sum_{i=1}^{N} I_{{\rm CM},i} = \sum_{i=1}^{N} (I_{{\rm T},i} + I_{{\rm B},i}) \tag{30}$$

as reported in (7) in the text.

[2]Otherwise, the hypothesis that the top nodes are not directly coupled to the system ground plane (i.e. that $\mathbf{Y}_{\rm TB} = -\mathbf{Y}_{\rm TT}$) would not be verified.

REFERENCES

[1] C. R. Paul, "Efficient Numerical Computation of the Frequency Response of Cables Illuminated by an Electromagnetic Field," in *IEEE Trans. Microwave Theory Tech.*, vol.22, no.4, pp. 454- 457, Apr 1974.

[2] J. W. Adams, J. Cruz, D. Melquist, "Comparison measurements of currents induced by radiation and injection," in *IEEE Trans. on Electr. Comp.*, vol.34, no.3, pp.360-362, Aug 1992.

[3] R. Khazaka, M. Nakhla, M., "Analysis of high-speed interconnects in the presence of electromagnetic interference," in *IEEE Trans. Microwave Theory Tech.*, vol.46, no.7, pp.940-947, Jul 1998.

[4] W. R. Eisenstadr, D. E. Bockelman, "Common and differential mode crosstalk characterization on the silicon substrate," in *IEEE Microwave and Guided Wave Letters*, vol.9, no.1, pp.25-27, Jan. 1999.

[5] C. H. Wu, C. H. Wang, C. H. Chen, "Novel Balanced Coupled-Line Bandpass Filters With Common-Mode Noise Suppression," in *IEEE Trans. Microwave Theory Tech.*, vol.55, no.2, pp.287-295, Feb. 2007.

[6] D. E. Bockelman, W. R. Eisenstadt, "Combined differential and common-mode scattering parameters: theory and simulation," in *IEEE Trans. Microwave Theory Tech.*, vol.43, no.7, pp.1530-1539, Jul. 1995.

[7] Road Vehicles - Component Test Methods - Part 4: Bulk Current Injection (BCI), ISO 11 452-4, Apr. 2002.

[8] Department of Defense Interface Standard, Requirements for the Control of EMI of Subsystems and Equipment, MIL-STD-461E, Aug 1999.

[9] N. J. Carter, The development of a revised susceptibility test for avionic equipment, in *Proc. IERE EMC Conf. Surrey*, U.K., Sept. 1982.

[10] S. Pignari, F. G. Canavero, "Theoretical assessment of bulk current injection versus radiation," in *IEEE Trans. on Electromagn. Compat.*, vol.38, no.3, pp.469-477, Aug 1996.

[11] S. Pignari, G. Spadacini, "BCI test conforming with statistical estimates of random-field radiation," in *Electr. Lett.*, vol.38, no.24, pp. 1499-1500, 21 Nov 2002

[12] A. Orlandi et al. "Equivalent Circuit Model of a Bundle of Cables for BCI Test," in *IEEE Trans. on EMC*, vol.48, no.4, pp.701-713, Nov. 2006.

[13] C. R. Paul, Analysis of Multiconductor Transmission Lines, 2nd. edition, Wiley Interscience, New York, 2008.

[14] A. Tsaliovich "Cable Shielding for Electromagnetic Compatibility", International Thomson Publishing (ITP), New York, 1995.

[15] "AD8362 50 Hz to 3.8 GHz 65 dB TruPwr Detector Datasheet", Rev. D, Analog Devices, Norwood, 2007.

[16] F-130A-1 Injection Current Probe Characterization, FCC, 2004

[17] F-51 Monitor Current Probe Characterization, FCC, 2004.

[18] P.S.Crovetti, F.Fiori, "A Critical Assessment of the Closed-Loop BCI Immunity Test Performed in Compliance With ISO 11452-4," in *IEEE Trans. on Instr. and Meas.*, vol.60, no.4, pp.1291-1297, Apr. 2011.

Paolo S. Crovetti (S'00, M'03) was born in Torino, Italy, in 1976. He received the Laurea and Ph.D. degrees in electronic engineering from the Politecnico di Torino in 2000 and 2003, respectively. Currently he is with the Department of Electronics, Politecnico di Torino, Italy, where he works as an Assistant Professor of Electronics. His main research interests are in the fields of analog integrated circuit analysis and design, electromagnetic compatibility (EMC), RF techniques and nonlinear circuits.

Franco Fiori (M'02) received the Laurea and the Ph.D. degrees in electronic engineering from the Polytechnic University of Torino, Italy in 1993 and 1997, respectively. From 1997 to 1998, he was a leader of the Electromagnetic Compatibility (EMC) Group, R&D Division, STMicroelectronics. In 1999, he joined the Electronics Department, Polytechnic University of Torino, where he is currently an associate professor of electronics. Since 2006, he has been a scientific leader of the Istituto Superiore Mario Boella, an advanced research institute on telecommunications based in Torino, Italy. He has authored or coauthored more than 100 papers published in international journals and conference proceedings. His current research interests include analog circuit analysis and design, nonlinear circuits, device modeling, and electromagnetic compatibility.